2. Mörz, M. (2022) A case report: acute myocardiadl infarction, coronal arteitis and myocarditis after BNT162b2 mRNA vaccination against COVID-19. In Preprints.
3. Bardosh, K., et al. (2020) COVID-19 vaccine boosters for young adults: a risk benefit assessment and ethical analysis of mandate politics at universities. In Journal of Medical Ethics. 0: 1-13.
4. CDC/NCHS-Morbidity and Mortality Weekly Report
5. Mohamed-Gabriel Almaeh, et al. (2012) Lipid nanopartyicles enhance the efficiency of mRNA and protein submit vaccines by ilnducing robust T follicular helper cell and humoral responses. In Immunity 54, 2877-2892.
6. Irrgang, P., et al. (2023) Irrgang, P. et al. (2023) Class switch toward noninflammatory, spike-specific IgG4 antibodies after reported SARS-CoV-2 mRNA vaccination. In Science Immunolorgy, 8. eade2798
7. Schmaling, M., Manniche, V., Ritis, P. (2023) Batch-dependent safety of the BNT162b2 mRNA COVID-19 vaccine. In European Journal of Clinical Investigation, Wiley & Sons Ltd, 53: e13998.
8. Oshima, N. et al. (1993) Development of image processing method for quantitative analysis of thrombus formation process in the microcirculation. In Journal of the Japanese Society of Biortheorogy (B&R) Volume 7 No. 2
9. Uversky, V.N. et al. (2023) IgG4 Antibodies induced by repeated vaccination may generate immune tolelance to the SARS-CoV-2 spike protein. In Vaccines (Basel), 11 (5): 991. doi:10.3390/vaccines 11050991.
10. Sato, K., et al. (2010) Neutralization of the SARS-CoV-2 Mu Mariant by Convalescent and Vaccine Serum. In The New England Journal of Medicine 385: 2397-2399.
11. Mori, T., et al. (2021) Elucidation of interaction regulating conformational satability and dynamics of SARS CoV-2 S-protein. In Biological Journal 120: 1060-1171.
12. AstraZeneca, Pfizer COVID vaccine anthibodies start declining after 10 weeks, says Lancet study. In Health, 2023.
13. Dorothea Bestle, et al. (2020) TMPRSS2 and furin are both essential for proteolyric activation of SARS-CoV-2 in human airway cells. In Life Science Alliance 3 (9): e202000786.
14. Йоичи Араи. Введение в клиническую токсикологию - COVID-19 вакцины токсчность, методы ее детоксикации и политическая цель ее производства. монография. Луцк : Вэжа-Друк. 2024. 366 с.
15. Йоичи Араи. Введение в Введение в вирусологию - Разрушительное и канцерогенное действие вакцин против COVID-19 на иммунную систему. монография. Луцк : Взжа-Друк. 2024. 278 с.
16. Shimizu, K. et al. (2021) Identification of TCR repertoires in functionally competent cytotoxic T cells cross-reactive to SARS-CoV-2. In Communications Biology 4: 1365.

# STRUCTURAL FEATURES OF APATITE-BASED COATINGS FOR MEDICAL IMPLANTS

**V.V. Nosenko[1], I.P. Vorona[1], A.M. Yaremko[1], V.M. Dzhagan[1], I.V. Zatovsky [2]**
[1] *V.E. Lashkaryov Institute of Semiconductor Physics, NAS of Ukraine, Kyiv*
[2] *F.D. Ovcharenko Institute of Biocolloidal Chemistry, NAS of Ukraine, Kyiv*
*e-mail: vvnosenko@ukr.net*

The interest in materials based on hydroxyapatite (HAP) is due to their wide application in the field of bioceramics (e.g., artificial bones and teeth), gas sensors, catalysis, etc. Important information about the nature of chemical bonds in these materials can be obtained using the Raman scattering method. In particular, vibrational spectroscopy is useful for studying the $PO_4^{3-}$ and $OH^-$ ions, which are structural units of HAP.

Experimental studies of the lattice dynamics of coatings for implants made of biocompatible HAPs by the Raman method (Fig. 1) revealed that in the spectra, in addition to the known bands of carbonate-containing HAP, features of unknown nature are also observed:

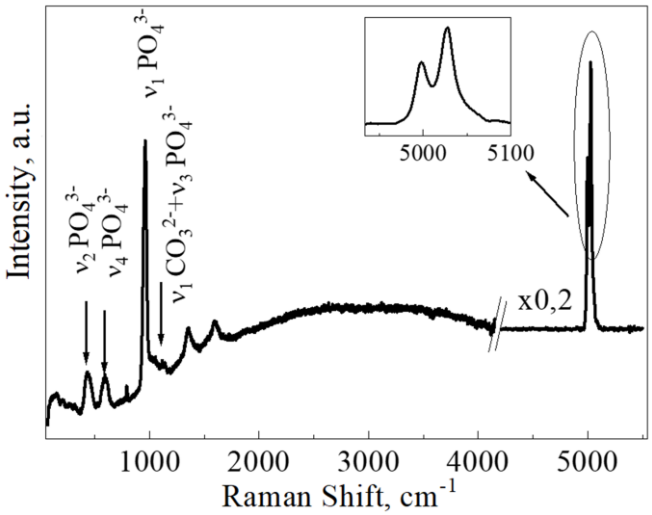


Fig. 1. Raman spectrum of the HAP coating.

- high-frequency bands with wave numbers of 5000 and 5027 cm$^{-1}$ of anomalously strong intensity (observed for the first time);

- a broad band in the range from ~1000 to 4000 cm$^{-1}$ with a maximum at ~2500 cm$^{-1}$; bands similar to it are called "background" in the literature, but there is no established interpretation of such bands.

To describe spectra of this material theoretically it was taken into account that in HAP ($Ca_{10}(PO_4)_6(OH)_2$) there is a large number of hydrogen bonds, which are characterized by high vibration

frequencies. To describe the broad band, the strong anharmonic interaction of the fundamental vibration of the hydrogen bond with low-frequency lattice phonons (Ω=134 $cm^{-1}$) was taken into account. Variation of the parameters $\gamma_{\mu}$ (damping constant), $\chi_{1,\mu}$ (coupling constant, which determines the number of phonons involved in the complex vibrational process) and $\delta_o$ (determines the shift of the theoretical spectrum) allowed us to describe the shape and position of the broad band and achieve good agreement between the model spectrum and the experimental one (Fig. 2). Thus, it is shown that the broad structureless Raman band is the result of the redistribution of the intensity of the *v* -OH band between phonon repetitions (at $\gamma_{\mu} > \Omega$). Based on the comparison of the calculations with the experiment, it was found that the frequency of the undisturbed fundamental *v*-OH vibration should be ~ 2530 $cm^{-1}$. This made it possible to interpret the experimentally observed spectral feature of ~ 5000 $cm^{-1}$ (Fig. 3) as an overtone of the *v*-OH vibration. To explain the unusually high intensity of the overtone band, anharmonic interaction (third-order anharmonicity, Γ≠0) between the fundamental *v*-OH vibration and its overtone was taken into account. Such an interaction is possible, since the most intense bands in the Raman spectra correspond to vibrations of complete symmetry and their overtones are also completely symmetric. Fig. 3 shows how an increase in the 3rd-order anharmonicity constant causes an increase in the intensity of the *v*-OH vibration overtone.

Another manifestation of anharmonic interaction in the spectra of HAP is the appearance of a doublet structure in the high-frequency region. It was described by the Fermi resonance of the

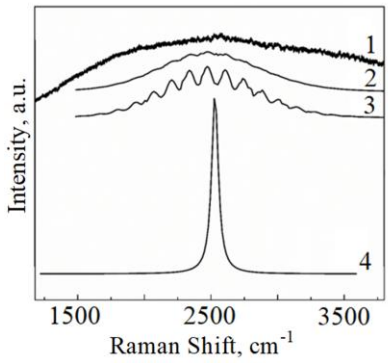


Fig. 2. Experimental Raman spectrum of HAP coating (1), (2-4) - theoretical spectra: $\chi_1$=2.4, $\gamma_\mu$=0.9 (2) or $\gamma_\mu$=0.6 (3). Reconstructed *v*-OH band (4).

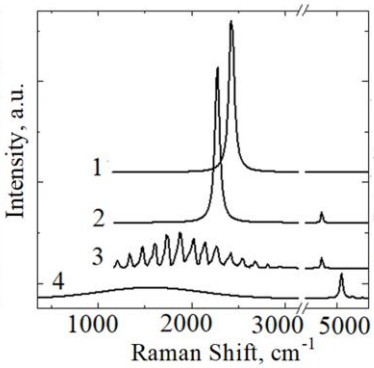


Fig. 3. The influence of the interaction of *v*-OH vibrations with phonons (constant $\chi_1$) and the anharmonicity constant Γ on the shape of model Raman spectra: Γ=0, $\chi_1$=0 (1); Γ=4, $\chi_1$=1 (2); Γ=4, $\chi_1$=4,5 (3); Γ=6, $\chi_1$=5 (4).

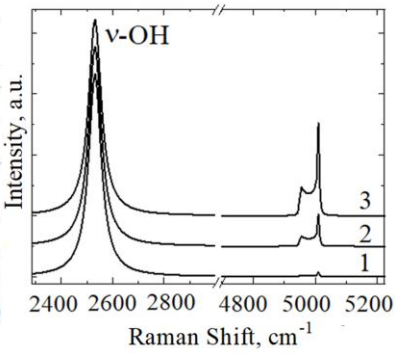


Fig. 4. The influence of the anharmonicity parameter β on the Raman spectra in the overtone region at Fermi resonance: β: 0.01(1); 0.1 (2); 0.2 (3).

fundamental vibration OH ($\nu_s$) and close to it in frequency the overtone of bending vibrations ($2\nu_b$) (Fig. 4).

Thus, the features of the Raman spectrum were theoretically explained as a result of the strong interaction between high-frequency vibrations of hydrogen bonds and low-frequency lattice phonons in crystals, taking into account the Fermi resonance interaction between the fundamental vibration OH ($\nu_s$) and the overtone of bending vibrations ($2\nu_b$), as well as the strong interaction of both components of the Fermi doublet with lattice phonons. Our Raman studies have highlighted the important role of both hydrogen bonds and strong anharmonic interaction between vibrations of different nature in the formation of the Raman spectrum of apatites.